Journal of Power Sources 196 (2011) 4468–4474

Contents lists available at ScienceDirect

Journal of Power Sources

journal homepage: www.elsevier.com/locate/jpowsour

# Electrocatalytic reduction of dioxygen on PdCu for polymer electrolyte membrane fuel cells

D.C. Martínez-Casillas[a], G. Vázquez-Huerta[a], J.F. Pérez-Robles[b], O. Solorza-Feria[a,*]

[a] Depto. de Química, Centro de Investigación y de Estudios Avanzados del IPN, A. Postal 14-740, C.P. 07360, México D.F., Mexico
[b] Depto. de Materiales, CINVESTAV-IPN, Libramiento norponiente 2000, Fracc. Real de Juriquilla, C.P. 76230 Santiago de Querétaro, Qro., Mexico

ARTICLE INFO

*Article history:*
Received 7 December 2010
Received in revised form 12 January 2011
Accepted 15 January 2011
Available online 26 January 2011

*Keywords:*
Oxygen reduction reaction
PdCu electrocatalyst
Electrocatalyst synthesis
PEMFC performance

ABSTRACT

The present research is aimed to study the oxygen reduction reaction (ORR) on a PdCu electrocatalyst synthesized through reduction of $PdCl_2$ and CuCl with $NaBH_4$ in a THF solution. Characterization of PdCu electrocatalyst was performed by X-ray diffraction (XRD), transmission electron microscopy (TEM) and energy-dispersive X-ray (EDX) spectroscopy. Characterization results showed that the synthesis method produced spherical agglomerated nanocrystalline PdCu particles of about 10 nm size. The electrochemical activity was evaluated using cyclic voltammetry (CV), rotating disc electrode (RDE) and electrochemical impedance spectroscopy (EIS) in a 0.5 M $H_2SO_4$ electrolyte at 25 °C. The onset potential for ORR on PdCu is shifted by ca. 30 mV to more positive values and enhanced catalytic current densities were observed, compared to that of pure Pd catalyst. The synthesized PdCu electrocatalyst dispersed on a carbon black support was tested as cathode electrode in a membrane–electrode assembly (MEA) achieving a power density of 150 mW $cm^{-2}$ at 0.38 V and 80 °C.



## 1. Introduction

The use of nanosized electrocatalysts within PEM fuel cells is highly desirable to reach the power density demanded by many applications based on renewable energy. Nanostructured catalysts are considered as an emerging field of interest which has opened new possible applications of novel materials for the advanced fuel cell industry [1–5]. Most of these advances are performed on materials formed by nanoparticles with enhanced properties compared to materials with the same chemical composition but made of much larger particles. There are different techniques for the synthesis of electrocatalysts. However, a basic requirement for nanomaterials synthesis is the uniformity of the final product in size, shape, and chemical composition [2,6]. Furthermore, the dispersion effect of the precious metal on the support will definitely influence the overall activity of the electrocatalyst. This is explained by the modification of the electronic environment of the catalyst particles together with the geometric effect, which could change the shape of the catalyst particles thus modifying the activity of the catalytic sites and the number of the active sites present in the electrode surface [4]. An important number of recent reports and reviews have been identified related to the current and short-term projected applications of modern nanotechnologies in polymer electrolyte membrane fuel cells (PEMFCs), because these offer several advantages such as improved energy efficiency and environmentally friendly power sources [2,4–7]. Main application areas include; transportation, distribution of energy and portable power systems. However, improving the sluggish kinetics of the cathodic reaction is critical in the development of these devices. This is due to the significant overpotential that cathode catalysts present, which is around 0.30 V even for the best electrocatalysts towards the oxygen reduction reaction (ORR). Therefore, this feature is one of the most important factors that limit the efficiency of the low temperature fuel cell. Current research efforts are focused on the development of catalysts to overcome this limitation through improved activities. Among various metals, nanosize palladium-based catalysts have attracted particular attention due to their special interaction with oxygen and high selectivity for water formation in a multielectron charge transfer process [8–12]. Some recent studies have reported that the combination of palladium with other metals, such as Ni [13–15], Fe[15], Sn [16], Rh [17] and Cu [18–22], synthesized by different methods, i.e., co-impregnation [15,18], colloidal synthesis [19], nanotubular mesoporous PdCu by galvanic replacement [20] and electrodeposition of PdCu [22], substantially improves the activity and stability of the alloys. This is attributed to the formation of bimetallic interactions which are stronger than a single metal–oxygen (M–O) interaction, thus generating a bimetallic material with greater stability. An interesting study reported that PdCu prepared using magnetron sputtering equipment [21] also presented enhanced catalytic activity for the ORR. This was

* Corresponding author. Tel.: +52 55 5747 3715; fax: +52 55 5747 3389.
*E-mail address:* osolorza@cinvestav.mx (O. Solorza-Feria).

0378-7753/$ – see front matter © 2011 Elsevier B.V. All rights reserved.
doi:10.1016/j.jpowsour.2011.01.050

attributed to a d band property that favored the ORR dissociative adsorption considered the rate-determining step during the ORR.

The aim of the present study is to compare in terms of the oxygen reduction reaction kinetics the incorporation of Cu to Pd produced by the borohydride chemical reduction route and to show how a synergistic effect can improve the stability and enhance the catalytic activity of the bimetallic compound. This method of synthesis allows the formation of PdCu nanoparticles at low-temperature, in a simple, economic and efficient way. In addition, the produced PdCu catalyst, as a continuation of our previous research [23], was used as a cathode material and tested in a polymer electrolyte membrane fuel cell. Furthermore, physical characterization of the electrocatalyst was performed using XRD, TEM and EDX techniques. The electrocatalytic activity of PdCu and the ORR mechanism were investigated by using steady-state techniques RDE and EIS. In addition, the performance of the membrane–electrode assembly (MEA) in a single PEM fuel cell was assessed using the PdCu as cathode and Pt as anode catalyst electrodes.

## 2. Experimental conditions

### 2.1. Electrocatalyst preparation

All chemicals were used as received and without further purifications. PdCu nanoparticles were synthesized by borohydride reduction of $PdCl_2$ (11.76 mM) and CuCl (12.0 mM) in dry THF, following the methodology reported elsewhere [16]. Briefly, chemicals were dissolved in 100 mL of dry THF maintaining vigorous stirring. 42.6 mM $NaBH_4$ was added as reducing agent. The reaction products were washed with distilled water and filtered. After filtration, the powder was dried and weighted thus obtaining a 95% yield.

### 2.2. Physical characterization

Crystal structure identification was performed by X-ray diffraction (XRD) using a D8 Advance diffractometer (Brucker) with monochromatic Cu Kα radiation ($\lambda = 1.54$ Å) in a $2\theta$ range from 30° to 90° with a step width of 0.02° $min^{-1}$. Pd and PdCu diffraction patterns were analyzed using MDI Jade 5.0 software to determine the crystallite size. Particle size, morphology and distribution of the material were assessed from results obtained by transmission electron microscopy (TEM) in a JEOL-2200FS operated at 200 kV, equipped with energy-dispersive X-ray (EDX) spectroscopy used to obtain an average and local chemical compositions of the sample. Electrocatalyst particle size was also calculated based on counting evaluation of a random selection of about 50 particles from each TEM image analyzed.

### 2.3. Electrochemical characterization

The oxygen reduction reaction was evaluated in a 0.5 M $H_2SO_4$ electrolyte saturated with oxygen for 30 min. Electrochemical experiments were performed in a conventional single-compartment three-electrode electrochemical cell. A platinum mesh was used as counter electrode and $Hg/Hg_2SO_4/H_2SO_4$ 0.5 M (MSE = 0.680 V/NHE) as reference electrode. The electrochemical experiments were performed on a potentiostat/galvanostat (PARSTAT model 2273). Cyclic voltammetry and rotating disk electrode experiments were carried out on a catalyst thin film deposited on a glassy carbon surface electrode ($A_{geom} = 0.126\ cm^2$) mounted on an interchangeable rotor RDE (Pine Instruments). The working electrode was prepared according to the methodology reported elsewhere [16]. PdCu thin film deposited on the glassy carbon electrode was prepared by the addition of 4 μL of a uniformly dispersed suspension resulting from the mixture of 40 μL of ethanol and 5 μL of Nafion® (5 wt.%, Du Pont 1000EW) and 1 mg PdCu (20 wt.%/C). The estimated amount of PdCu catalyst on the glassy carbon electrode surface was about 0.14 mg $cm^{-2}$. The rotation rate of the working electrode was in the range of 100 and 1600 rpm at 5 mV $s^{-1}$. The cyclic voltammetry (CV) characterization of the working electrode was performed in nitrogen-purged 0.5 M $H_2SO_4$ solution at room temperature. Prior to CV experiments the electrode was subjected to 20 cycles in the range of 0.0–1.2 V/NHE, in order to remove oxides and impurities on the electrode surface and obtain reproducibility during the CV experiments.

The ORR activity was measured in oxygen saturated acid solution at room temperature and during the measurement a moderate oxygen gas flow was maintained above the electrolyte. The electrical impedance spectra were obtained immediately after the application of a potential step ($E$) of 180 s, the characterization was performed at the desired value of $E$. The amplitude of the ac signal perturbation was 10 mV. The frequency range scanned was from 100 kHz to 10 mHz. During experiments, the working electrode was rotated at 1000 rpm. The potential step and electrode rotation are necessary in order to establish a pseudo steady-state condition before impedance data acquisition. The impedance spectra were obtained using different values of $E$ between 0.78 V and 0.38 V/NHE.

### 2.4. Preparation and characterization of the membrane–electrode assembly

A three layered structure, diffusion, catalyst and monomer layers, was used to prepare the membrane–electrode assembly (MEA). Nafion® 117 (Dupont Fluoro Products) was used as a polymer electrolyte membrane, which was treated by consecutive boiling processes for 1 h in 3% $H_2O_2$, 2 M $H_2SO_4$ and deionized water, according to the procedure previously described [3,24]. Before spraying, membranes were dried and flattened. Cathodic catalytic inks were prepared by mixing and sonicating a suspension formed by the PdCu electrocatalysts, Vulcan carbon, Nafion ionomer and ethanol. The commercial electrode (1 mg 20 wt.% Pt/C, E-TEK Electrochem) was used in the anode side of the assembly. Each MEA was prepared by spraying the corresponding catalyst ink on the cathodic side of the pretreated 117 Nafion membrane. The catalyst loading at the cathode side was about 0.8 $mg_{PdCu}\ cm^{-2}$. The MEA was prepared by placing the gas diffusion layer (carbon cloth) above the electrode at the cathodic side and the commercial electrode at the anodic side of the 117 Nafion membrane, followed by hot-pressing of the assembly at 120 °C and 11 kg $cm^{-2}$ for 1 min. The effective electrode area for the anode and cathode sides was 5 $cm^2$. The MEAs were tested with a commercial fuel cell system (Compucell GT, Electrochem 890B) in a single cell rig with 5 $cm^2$ of geometrical area. The gas pressures at the anode and cathode sides were kept at 30 psi for $H_2$ and 30 psi for $O_2$, respectively. The fuel cell test station was operated with high purity $H_2$ and $O_2$ at 100 $cm^3\ min^{-1}$. Humidification of reactant gases was kept at 5 °C above the temperature of the cell. The performance was measured under steady-state conditions from 25 to 80 °C.

## 3. Results and discussion

### 3.1. Physical characterization

X-ray diffraction pattern of PdCu synthesized by borohydride chemical reduction method is shown in Fig. 1. The diffraction pattern shows at least five diffraction peaks which neither matches to Pd nor Cu reported on standard JCPDS cards (Pd, 65-2867), (Cu, 04-0836), respectively. This indicates the formation of a new sin-

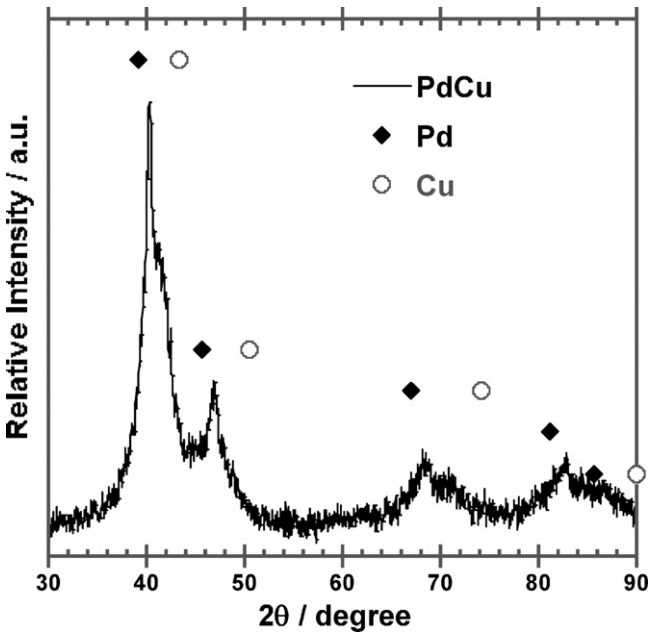


**Fig. 1.** XRD spectra of PdCu electrocatalyst.

gle bimetallic phase. PdCu peaks are associated with the formation of strong interactions between the Pd and Cu atoms, which also results in an increased stability of this catalyst with respect to Pd. A broad feature in the low angle scattering region suggests that nanocrystallites with a few nanometers in diameter are embedded in an amorphous product. Nanocrystallites were about 27% as determined using MDI Jade 5.0 software. Fitting of the diffraction PdCu catalyst pattern using the academic Topas software resulted in an average crystallite size of about 11 nm.

Fig. 2a shows a TEM image of agglomerated particles containing small homogeneous particles in nanometric size with spherical morphology. The histogram in Fig. 2b, indicates a particle size distribution with values ranging from 8 to 11 nm, which is in agreement with results obtained from XRD data of Fig. 1. The inset in Fig. 2a shows the corresponding selected area of diffraction patterns. These particles were analyzed by EDX, results indicate an atomic Pd/Cu ratio of 1.1 in the sample. TEM mapping images for the PdCu sample, Fig. 3, shows a uniform elemental Cu and Pd distribution in the particle of the mapped area. Therefore, these results agree with those reported for typical electrocatalyst analysis, and suggest that the PdCu nanocrystallite synthesis method is suitable for a cathode catalyst material.

### 3.2. Electrochemical characterization

Fig. 4 shows the final cycle of cyclic voltammetry. 20 cycles were used for cleaning and activation of Pd and PdCu samples. These voltammograms indicate the typical behavior of Pd distinguishing the proton adsorption–desorption peaks of hydrogen presented in the potential range of 0.0 V–0.35 V/NHE. Hydroxide adsorption and reduction are different from those reported for Pd alone [16]. There is a favored $OH_{ad}$ on the PdCu electrocatalyst and this is attributed to the presence of the second metal which also shifts the oxygen reduction potential from about 0.03 V to a more positive value. An increase in the cathodic current density at 0.7 V/NHE is associated to the elevated concentration of anions previously adsorbed and reduced at this electrode potential, this indicates that the PdCu electrocatalyst possesses a higher oxygen adsorption capacity than Pd alone.

Due to the low oxygen solubility in acid media, the oxygen reduction reaction, ORR, depends strongly on hydrodynamic conditions. The ORR characteristic set of polarization curves from RDE measurements, at different rotation rates, of nanometric PdCu/C dispersed is summarized in Fig. 5a . During the electrochemical reactions, the charge transfer and the mass transfer are two consecutive processes that could define the rate determining step, depending on its relative rate. From polarization curves both processes are distinguished. At the beginning of the scan potential in the negative direction from the open circuit potential, 0.90 V/NHE, at low overpotential a defined charge transfer control is observed in the region where the current density is independent of the electrode rotation speed. The mixed kinetic-diffusion control region (−0.8 to −0.7 V/NHE) is followed by the appearance of a diffusion limiting current region. With increase of the rotation rate, currents also are raised due to an enhancement of the oxygen diffusion through the thin film electrode surface. According to these behaviors, the overall measured current of the oxygen reduction can be considered as been dependent on the kinetic current density, $j$, the diffusion-limited current density, $j_L$, and the diffusional current density in the Nafion film, $j_f$. This diffusional current density can be considered not significant when it is applied as very thin

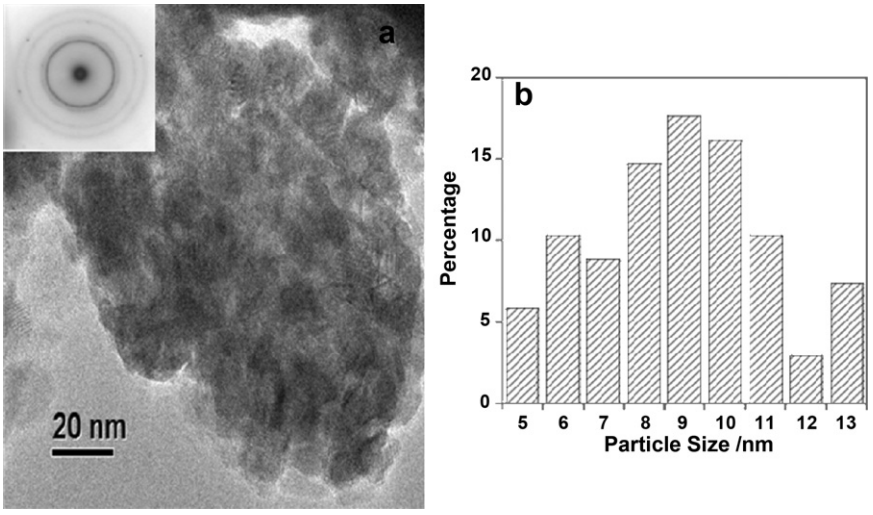


**Fig. 2.** (a) TEM image of: as-synthesized PdCu electrocatalysts. Electron diffraction is inset showing a diffuse cubic pattern. (b) Particle size histogram.

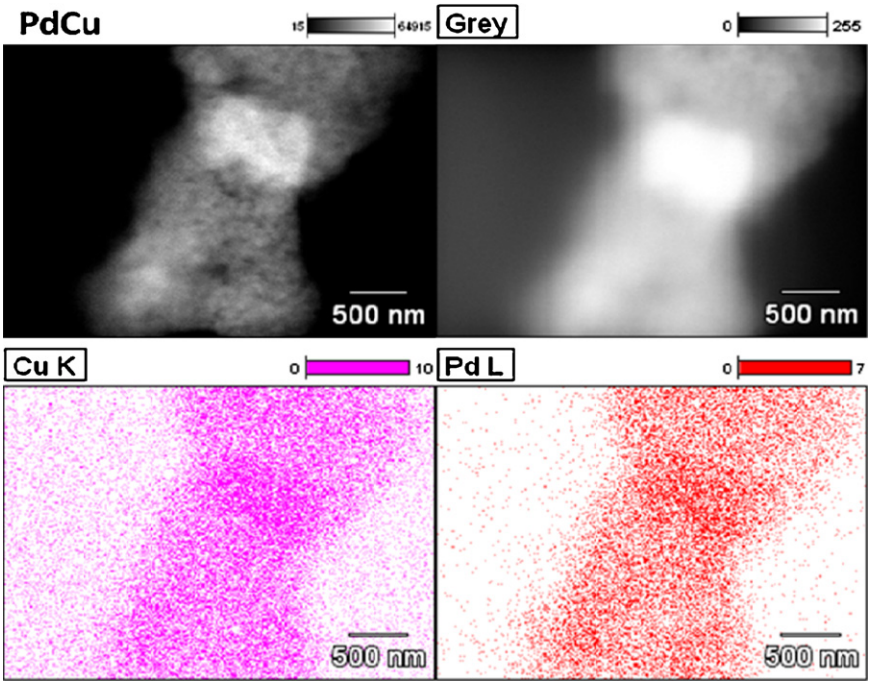


**Fig. 3.** TEM mapping images for the as-synthesized PdCu electrocatalyst sample.

film, which is the case on the present study (1 μL at 5 wt.% Nafion in 8 μL of solution), according to the Eq. (1) [25].

$$\frac{1}{j} = \frac{1}{j_k} + \frac{1}{j_L} + \frac{1}{j_f} = \frac{1}{j_k} + \frac{1}{B\omega^{1/2}} \quad (1)$$

Fig. 5b shows a plot of the inverse of the overall current density, $j^{-1}$, as function of the inverse square root of the rotating speed, $\omega^{-1/2}$, known as the Koutecky–Levich plot. This graph shows a linear relationship between $j^{-1}$ and $\omega^{-1/2}$, which indicates a first order kinetics of the PdCu with respect to the oxygen reduction reaction within the potential range studied. The experimental average slope value, $B_{exp} = 8.40 \times 10^{-2}$ mA cm$^{-2}$ rpm$^{-1/2}$ was in agreement with the theoretical slope, $B_{th} = 10.65 \times 10^{-2}$ mA cm$^{-2}$ rpm$^{-1/2}$, calculated for the four-electron transfer process leading to water formation, i.e., $O_2 + 4H^+ + 4e^- \rightarrow 2H_2O$. The kinetic current is proportional to the intrinsic properties of the catalyst, the catalytic activity of a material can be measured in terms of parameters deduced from the mass transfer-corrected Tafel slope. Fig. 5c shows the mass-transfer-corrected Tafel plot for the PdCu, nanometric Pd and Pt electrocatalysts included for comparison in an oxygen-saturated 0.5 M $H_2SO_4$ solution deduced from Fig. 5a and using Eq. (2).

$$j_k = \frac{jj_L}{j_L - j} \quad (2)$$

Electrocatalytic response of the Tafel slope of each electrocatalyst shows a linear behavior at high current density from which

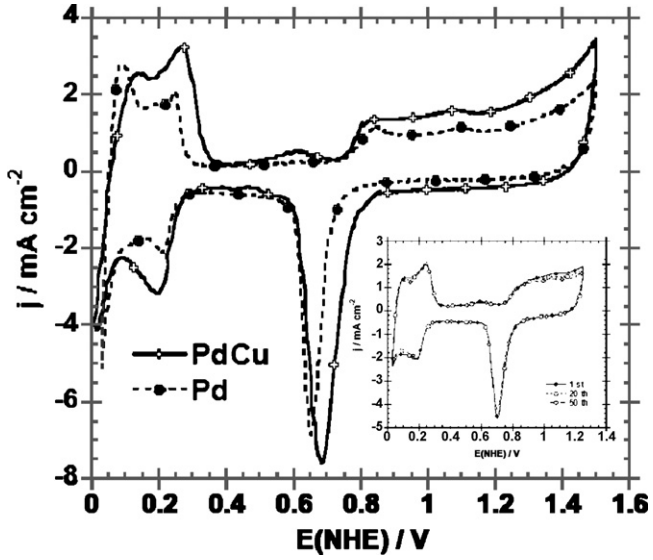


**Fig. 4.** Cyclic voltammogram of Pd and PdCu catalyst in 0.5 M $H_2SO_4$, bubbled with $N_2$ for 15 min, at 25 °C. Scan rate, 100 mV s$^{-1}$. Inset, cyclic voltammograms of PdCu corresponding to 1st, 20th and 50th cycles at 100 mV s$^{-1}$.

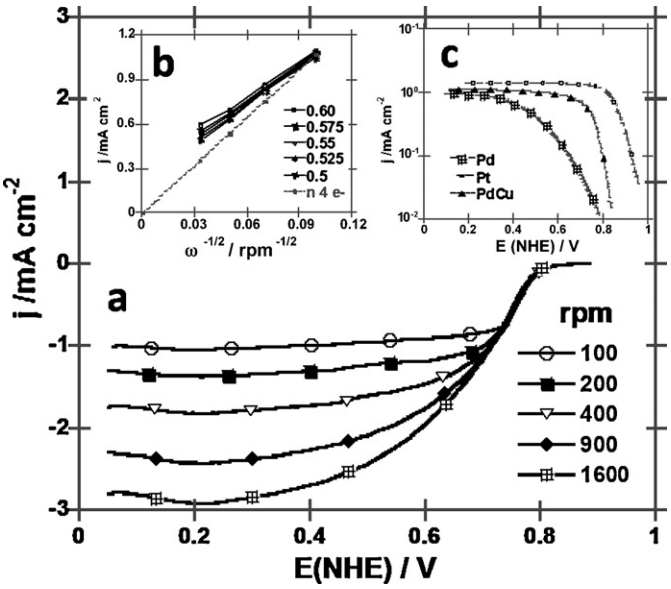


**Fig. 5.** (a) Steady-state polarization curves for the ORR on PdCu in 0.5 M $H_2SO_4$. (b) Koutecky–Levich treatment and (c) mass-transfer corrected Tafel plots on Pd and PdCu electrocatalysts.

**Table 1**
Open circuit potential, Tafel slope ($b$), charge transfer coefficient ($\alpha$) and exchange current density ($j_0$) of the ORR on Pt, Pd and PdCu, in 0.5 M $H_2SO_4$. Kinetic parameters $b$, $\alpha$ and $j_0$ were obtained from RDE and EIS data.

| Material | $E_{ocp}$ (mV) | $-b$ (V dec$^{-1}$) | $\alpha$ | $j_0$ (mA cm$^{-2}$) |
|---|---|---|---|---|
| Pd | 0.80 | 0.125 | 0.47 | $3.00 \times 10^{-6}$ |
| $PdCu_{RDE}$ | 0.86 | 0.098 | 0.60 | $5.71 \times 10^{-6}$ |
| $PdCu_{EIS}$ | 0.86 | 0.096 | 0.61 | $4.64 \times 10^{-6}$ |
| Pt | 0.95 | 0.120 | 0.49 | $5.06 \times 10^{-4}$ |

kinetic parameters were obtained. A shift of 60 mV to cathodic direction of the open circuit potential and an enhancement of the catalytic activity are observed on PdCu. The kinetic parameters deduced from the analysis of the Tafel slope at high overpotential are summarized in Table 1. It is well known that the rate of the cathodic reaction is proportional to the exchange current density and exponentially related to the Tafel slope. It is desirable to minimize the Tafel slope in order to achieve a high voltage for high operating current density. The deduced Tafel slope, $b$, of the nanometric PdCu is lower than that of Pd, indicating that the bimetallic catalyst exhibits a better catalytic activity for the same ORR, attributed to the bifunctional effect in which the catalytic properties of each of the elements combine in a synergetic form to yield a more active surface than Pd and Cu alone.

The impedance spectra of PdCu/C in $O_2$-saturated 0.5 M $H_2SO_4$ solution are shown in Fig. 6, two behaviors which depend on $E$ are observed. In this figure, for $E > 0.48$ V vs NHE, the Nyquist and Bode plots present a single time constant (Fig. 6a and b) associated to a single process. In Fig. 6a, real and imaginary components of impedance diminish as the potential becomes more negative; however, the curves always show a single time constant in this potential range. In contrast, for $E < 0.48$ V, distorted semicircles are distinguished in Nyquist spectra (Fig. 6c), this indicates that more than one process is present. Bode diagrams in this potential range

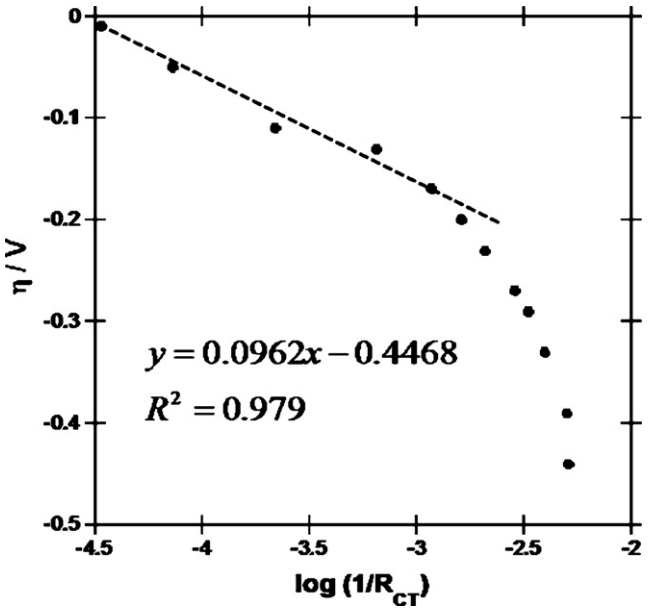


**Fig. 7.** Variation of overpotential ($\eta$) vs $\log 1/R_{CT1}$ of the ORR on PdCu/C, in $O_2$ – saturated 0.5 M $H_2SO_4$ electrolyte.

also present two time constants (Fig. 6d), the first time constant is observed at middle frequencies, while the second one is in the low frequency range. The semicircles depicted in Fig. 6a are associated with a multielectron charge transfer process, from $O_2$ to $H_2O$ formation. This latter has been reported in several works using Pd and Pd-based electrocatalysts [26–28]. Moreover, it has been reported that $H_2O_2$ generation depends on the applied potential. Detection of $H_2O_2$ has been reported for different materials (i.e., Hg, Cu, Pd,

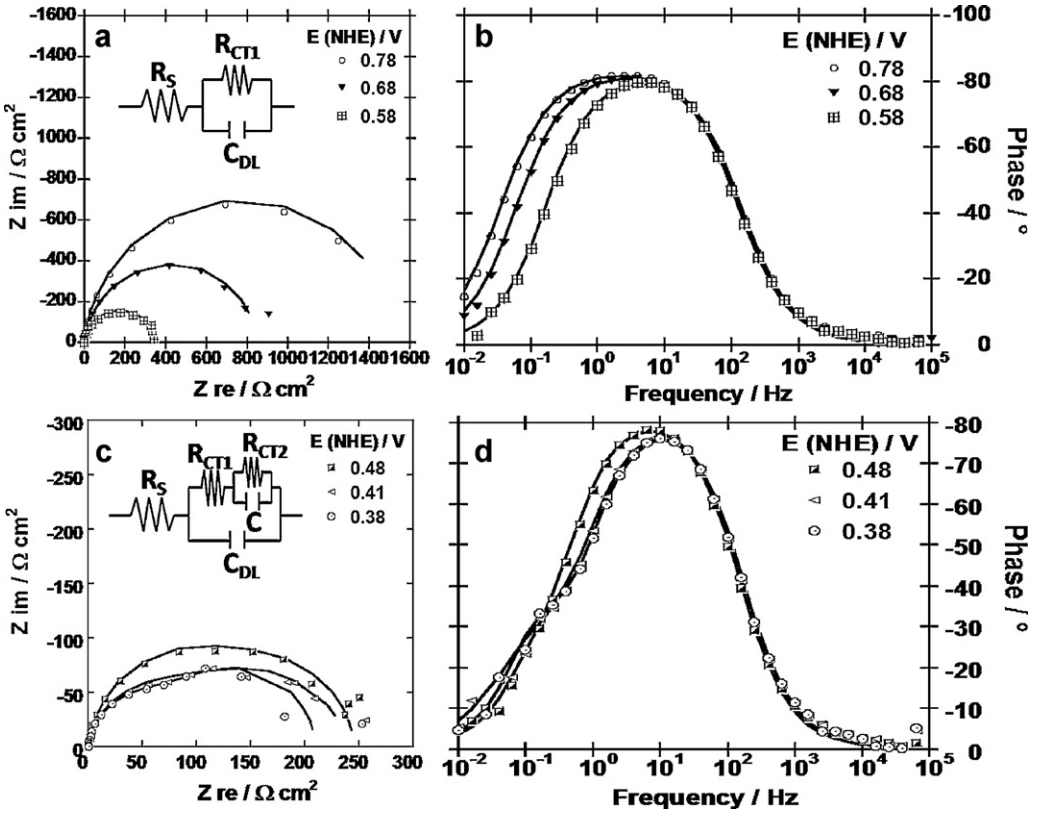


**Fig. 6.** Nyquist and Bode diagrams of the ORR on PdCu/C (catalyst loading of 0.14 mg cm$^{-2}$) in $O_2$ – saturated solution of 0.5 M $H_2SO_4$ using different potentials. Spectra in lines belong to calculated spectra constructed from the fitted values using the corresponding electric circuit in the figure.

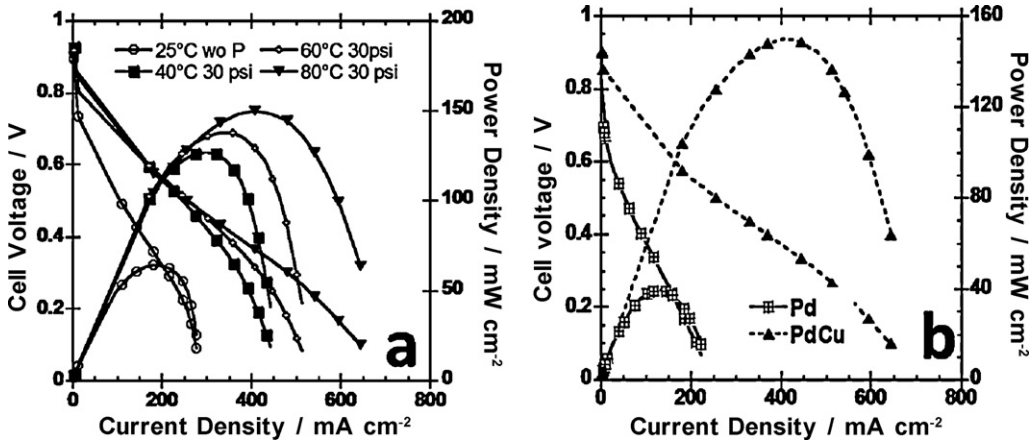


**Fig. 8.** (a) Single fuel cell performance curve of Pt (10 wt.%)/C (E-TEK), with a catalyst loading of 0.8 mg cm$^{-2}$ as anode and PdCu (20 wt.%)/C with catalyst loading of about 0.14 mg cm$^{-2}$ as cathode. The fuel cell was operating with $H_2/O_2$ at different temperatures. (b) Comparison of Pd and PdCu performances at 80 °C.

$Pd_{80}Co_{20}$ and $Au_{60}Co_{40}$) [29,30] tested as catalysts for the ORR, in 0.5 M $H_2SO_4$. All these materials presented values of transferred electrons, $n$, between 2 and 4.

The materials showed intermediate values (i.e., 2–4) of transferred electrons as a function of potential. The quantity of $H_2O_2$ can be related to the total number of electrons, $n$, with $n = 2$ only $H_2O_2$ is generated, while $n = 4$ indicates $H_2O$ formation. The intermediate values of $n$, between 2 and 4 may be associated to the formation of intermediate species such as $OH_{ads}$ and $O_2H_{ads}$. In the present work, the second time constant is associated to the reduction of the $H_2O_2$ generated; it is assumed that $H_2O_2$ is the main intermediate during the ORR.

In order to obtain quantitative information from the impedance spectra, the electric circuits in Fig. 6a and b were employed to fit the impedance diagrams. In Fig. 6, $R_S$ represents the resistance of the solution, $C_{DL}$ is related with the capacitance of the double layer, $R_{CT1}$ is the charge transfer resistance of the reduction process from $O_2$ to $H_2O$, and $R_{CT2}$ is the charge transfer resistance associated to the reduction process from $H_2O_2$ to $H_2O$. $C$ represents the capacitance of all absorbed intermediates. The fit of the impedance spectra and the corresponding electric circuit was performed by using the Boukamp's software [31], the results are shown in Fig. 6, the electric circuit inset in this figure allows good fitting ($\chi^2 \sim 10^{-3}$). The values for all elements in the circuits were obtained, however only the values of $R_{CT1}$ are shown. The $R_{CT1}$ values obtained from the fit can be used to determine the ORR kinetic parameters. Fig. 7 shows the behavior of $\eta = E - E_{ocp}$ vs $\log 1/R_{CT1}$, ($E_{ocp}$ is the open circuit potential ~0.86 V vs NHE). The values of $b$ and $\alpha$ following this procedure are summarized in Table 1. The values of $b$ and $\alpha$ by using RDE and EIS data are in good agreement with each other (Table 1), this latter shows that EIS measurements can be a powerful tool for obtaining the ORR kinetics parameters. The electrocatalytic behavior of PdCu, shown above, indicates that this material should be considered as a candidate to be used as cathodic electrode in a PEMFC.

### 3.3. Performance of membrane–electrode assemblies, MEAs

MEAs were prepared by spraying catalyst ink on the cathodic side of a pretreated Nafion® 117 membrane. Then, the catalyzed membrane was sandwiched between porous carbon cloth (cathode side) and commercial platinum carbon cloth (Pt/C, E-TEK, 20 wt.% with a loading of 0.5 mg cm$^{-2}$) for the anode. MEA was inserted into the fuel cell for testing. In order to study the temperature effect on the MEA performance, curves of cell voltage and power density vs current density were recorded at 25, 40, 60 and 80 °C. The fuel cell was fed with $H_2/O_2$ under 30/30 psi pressure. Fig. 8a shows the fuel cell performance at different temperatures using PdCu as cathodic catalyst. An improvement of MEA performance with the increase of the operating temperature was observed. Open circuit voltages, $E_{oc}$, were around 0.95 V at the operating temperature. The maximum power density, $W_{max}$, was 125 mW cm$^{-2}$ at 40 °C, increasing to 150 mW cm$^{-2}$ at 80 °C, almost 17% higher than the starting current. This behavior indicates that the oxygen reduction on PdCu catalyst is activated by temperature. The power density obtained with PdCu catalyst is higher than that obtained with palladium alone (Fig. 8b), under the same experimental conditions. While the result of power density with PdCu catalyst is lower than that obtained with commercially available platinum E-TEK (results not shown) the relatively low output performance observed with the bimetallic catalyst may be attributed to the amorphous phase mixed with the nanocrystallites of PdCu. Additional effort in catalyst preparation and assembly characterizations should be carried out to optimize the fuel cell operation.

## 4. Conclusions

Bimetallic PdCu nanoparticles with a crystallite size of 11 nm were synthesized following the borohydride reduction method. EIS diagrams of PdCu/C present one or two time constants depending on the applied $E$. The first time constant of impedance spectra was associated to the reduction process from $O_2$ to $H_2O$, while the second one to the reduction of $H_2O_2$ to $H_2O$. Performance of $H_2/O_2$ PEM single cell, using PdCu/C (20 wt.%/C) with a loading of about 0.14 mg cm$^{-2}$ as cathodic catalyst and Pt/C (E-TEK, 20 wt.% with a loading of 0.5 mg cm$^{-2}$) as anode, showed a maximum power density, $W_{max}$, of 125 mW cm$^{-2}$ at 40 °C, increasing to 150 mW cm$^{-2}$ at 80 °C, almost 17% higher than the starting current.

## Acknowledgments

We gratefully acknowledge the support of the Mexico's National Council of Science and Technology, CONACYT, under grants 83247 and 101537. DCMC thanks CONACYT for the doctoral fellowship. GVH thanks ICYTDF for the financial support through a postdoctoral grant. The authors acknowledge Dr. Paz del Angel from the IMP for the TEM measurements.

## References

[1] A.A. Gewirth, M.S. Thorum, Inorg. Chem. 49 (2010) 3557.
[2] Y. Li, A. Somorjai, Nano Lett. 10 (2010) 2289.
[3] J.J. Salvador-Pascual, V. Collins-Martínez, A. López-Ortíz, O. Solorza-Feria, J. Power Sources 195 (2010) 3374.

[4] E. Antolini, Appl. Catal. B: Environ. 88 (2009) 1.
[5] R. Ferrando, J. Jellinek, R.L. Johnston, Chem. Rev. 108 (2008) 845.
[6] V. Neburchilov, H. Wang, J.J. Martin, W. Qu, J. Power Sources 195 (2010) 1271.
[7] D. Vollath, Nanomaterials: An introduction to Synthesis, Properties and Applications, Willey-VCH, Weinheim, 2008.
[8] H. Liu, A. Manthiram, Energy Environ. Sci. 2 (2009) 124.
[9] B. Li, J. Prakash, Electrochem. Commun. 11 (2009) 1162.
[10] G. Vázquez, O. Solorza-Feria, J. New Mater. Electrochem. Syst. 12 (2009) 17.
[11] M. Shao, P. Liu, J. Zhang, R. Adzic, J. Phys. Chem. B 111 (2007) 6772.
[12] K. Lee, O. Savadogo, A. Ishihara, S. Mitsushima, N. Kamiya, K. Ota, J. Electrochem. Soc. 153 (2006) A20.
[13] J. Zhao, A. Sarkar, A. Mantiram, Electrochim. Acta 55 (2010) 1756.
[14] G. Ramos-Sánchez, H. Yee-Madeira, O. Solorza-Feria, Int. J. Hydrogen Energy 33 (2008) 3596.
[15] X. Wang, N. Kariuki, S. Niyogi, M. Smith, D.J. Myers, ECS Trans. 16 (2008) 109.
[16] J.J. Salvador-Pascual, S. Citalán-Cigarroa, O. Solorza-Feria, J. Power Sources 172 (2007) 229.
[17] Z. Bai, L. Yang, J. Zhang, L. Li, J. Lv, C. Hu, J. Zhou, Catal. Commun. 11 (2010) 919.
[18] X. Wang, N. Kariuki, J.T. Vaughey, J. Goodpaster, J. Kumar, D.J. Myers, J. Electrochem. Soc. 155 (2008) B602.
[19] N.N. Kariuki, X. Wang, J.R. Mawdsley, M.S. Ferrandon, S.G. Niyogi, J.T. Vaughey, D.J. Myers, Chem. Mater. 22 (2010) 4144.
[20] C. Xu, Y. Zhang, L. Wang, L. Xu, X. Bian, H. Ma, Y. Ding, Chem. Mater. 21 (2009) 3110.
[21] F. Fouda-Onana, S. Bah, O. Savadogo, J. Electroanal. Chem. 636 (2009) 1.
[22] F. Gobal, R. Arab, J. Electroanal. Chem. 647 (2010) 66.
[23] D.C. Martínez-Casillas, O. Solorza-Feria, ECS Trans. 20 (2009) 275.
[24] K. Suárez-Alcántara, O. Solorza-Feria, Fuel Cells 10 (2010) 84.
[25] A.J. Bard, L. Faulkner, Electrochemical Methods: Fundamentals and Applications, Wiley, New York, 2001, p. 341.
[26] W. Wang, D. Zheng, Ch. Du, Z. Zou, X. Zhang, B. Xia, H. Yang, D.L. Akins, J. Power Sources 167 (2007) 243.
[27] R.G. González-Huerta, A. Chávez-Carvayar, O. Solorza-Feria, J. Power Sources 153 (2006) 11.
[28] D.C. Martínez-Casillas, G. Vázquez-Huerta, J.F. Pérez-Robles, O. Solorza-Feria, J. New Mater. Electrochem. Syst. 13 (2010) 163.
[29] C.M. Sánchez-Sánchez, A.J. Bard, Anal. Chem. 81 (2009) 8094.
[30] G. Vázquez-Huerta, G. Ramos-Sánchez, A. Rodríguez-Castellanos, D. Meza-Calderón, R. Antaño-López, O. Solorza-Feria, J. Electroanal. Chem. 645 (2010) 35.
[31] B.A. Boukamp, Solid State Ionics 20 (1986) 31.